Acta Mechanica Sinica
https://doi.org/10.1007/s10409-021-01067-1

RESEARCH PAPER

On the electrophysiology of the atrial fast conduction system: an uncertain quantification study

Giulio Del Corso[1] · Roberto Verzicco[1,2,3] · Francesco Viola[1]

Received: 22 October 2020 / Revised: 20 January 2021 / Accepted: 28 January 2021

Abstract
Cardiac modeling entails the epistemic uncertainty of the input parameters, such as bundles and chambers geometry, electrical conductivities and cell parameters, thus calling for an uncertainty quantification (UQ) analysis. Since the cardiac activation and the subsequent muscular contraction is provided by a complex electrophysiology system made of interconnected conductive media, we focus here on the fast conductivity structures of the atria (internodal pathways) with the aim of identifying which of the uncertain inputs mostly influence the propagation of the depolarization front. Firstly, the distributions of the input parameters are calibrated using data available from the literature taking into account gender differences. The output quantities of interest (QoIs) of medical relevance are defined and a set of metamodels (one for each QoI) is then trained according to a polynomial chaos expansion (PCE) in order to run a global sensitivity analysis with non-linear variance-based Sobol' indices with confidence intervals evaluated through the bootstrap method. The most sensitive parameters on each QoI are then identified for both genders showing the same order of importance of the model inputs on the electrical activation. Lastly, the probability distributions of the QoIs are obtained through a forward sensitivity analysis using the same trained metamodels. It results that several input parameters—including the position of the internodal pathways and the electrical impulse applied at the sinoatrial node—have a little influence on the QoIs studied. Vice-versa the electrical activation of the atrial fast conduction system is sensitive on the bundles geometry and electrical conductivities that need to be carefully measured or calibrated in order for the electrophysiology model to be accurate and predictive.

Keywords Uncertainty quantification · Global sensitivity analysis · Forward analysis · Atrial modelling · Electrophysiology · Monodomain model

1 Introduction

At each heartbeat the synchronized contraction of the cardiac chambers is originated by the timely electrical activation of the myocytes that are integrated in a sophisticated and robust electrical network. As sketched in Fig. 1a, the local myocytes depolarization starts from the sinoatrial node (SA-node hereafter), which is located in the right atrium at the junction of the crista terminalis close to the entrance of the superior vena cava, and then propagates across the atria. When a myocyte is reached by the electrical propagation front, the local transmembrane potential rapidly changes from the negative potential (of about −85 mV) to a positive value (of about 20 mV) before returning to the resting negative potential after about 300 ms, see Fig. 1b. The propagation of the electrical depolarization front is affected by the strong heterogeneity of the cardiac tissue, with an average conduction velocity of about 0.3–0.5 m/s in the atrial fibers that reaches 1.5–2 m/s in specialized high conductivity structures, the so-called internodal pathways [1,2]. These (i) anterior internodal, (ii) middle (Wenckbach) and (iii) posterior (Thorel) bundles connect the SA-node to the left atrium (through the Bachmann's bundle) and to the atrioventricular node (AV-node hereafter), thus ensuring a rapid and smooth conduction across the whole heart. The AV-node connects the atrial to the ventricular electrical network and is made by specialized cardiac cells designed to slow down the electrical propagation by an AV-delay of about 90 ms [1], which plays a crucial role for the

Executive Editor: Ji-Zeng Wang

✉ Francesco Viola
francesco.viola@gssi.it

[1] GSSI (Gran Sasso Science Institute), L'Aquila, Italy

[2] University of Roma Tor Vergata, Rome, Italy

[3] POF Group, University of Twente, Enschede, The Netherlands

Published online: 19 March 2021

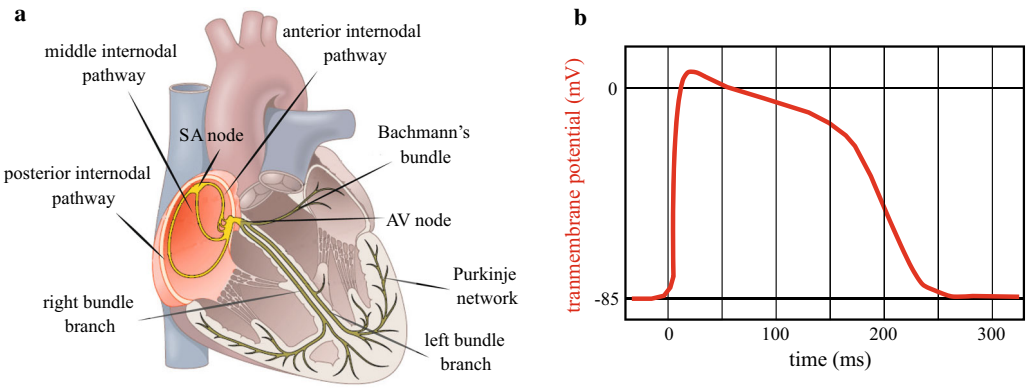

Fig. 1 **a** Sketch of the electrical network of the heart adapted from Ref. [1], with highlighted the atrial components. **b** Sketch of a typical depolarization/polarization cycle (action potential) of an atrial myocyte [1]

cardiac dynamics as it ensures a timely atrial contraction before the ventricular one. The AV-node is thus the electrical connection between the atrial and the ventricular bundle network: the propagation front travelling across the AV-node to the bundle of His further propagates through the Purkinje network at a higher conduction speed of about 4 m/s [1], thus allowing for an almost simultaneous activation of the ventricular muscle.

The state-of-the-art model for simulate and study the electrical activation within the heart chambers in healthy and pathological conditions is the bidomain model [3,4], which is called in this way because the conductive myocardium is modeled as an intracellular and an extracellular overlapping continuum media separated by the myocytes membranes [5]. The resulting system of reaction–diffusion partial differential equations governs the electrical propagation across the myocytes and is coupled with the cellular ionic model (given by a set of ordinary differential equations) describing the current flows through the ion channels. In the case the extracellular and intracellular conductivity tensors are parallel to each other, as is always the case in monodimensional domains, the bidomain equations can be simplified as a single governing equation for the transmembrane potential, the monodomain system. The latter is computationally cheaper not only because the number of degrees-of-freedom is reduced but also because the equations are more stable numerically [3]. In contrast with computationally cheaper electrophysiology models such as the eikonal [6] method that correctly solve the electrical propagation through the medium, the monodomain/bidomain model is also seen to accurately reproduce cardiac phenomena including ischemic events and defibrillation.

Cardiac modelling, however, entails a high epistemic uncertainty for the geometrical and electrical input parameters entering in the governing equations as only some of these quantities can be measured in-vivo. The calibration of electrical input parameters for monodomain equations based on available medical data is typically solved in the framework of monodomain inverse conductivity problem (MICP). Multiple techniques, including variational data assimilation procedure [7] and proper generalized decomposition (PGD) [8], were used to derive space-dependent conductivity for 2D and 3D media. The input parameters variability among individuals can be rigorously accounted for through an uncertainty quantification (UQ) approach, where the input parameters are treated as aleatory variables with an uncertainty probability distribution function (PDF). Consequently, not a single simulation but a set of simulations is run in order to determine the sensitivity of some quantities of interest (QoIs) on the input parameters (and their PDFs) as well as the PDFs of the QoIs. This statistical approach has been recently used by the authors to investigate the propagation of uncertainties in an electrophysiology model for the electrical activation of the left ventricular myocardium [9].

In this work we study the global sensitivity of the electrical activation within the atrial fast conduction network on the geometry and on the electrical properties of the system. The aim is to isolate which of the model parameters, either geometrical or electrical, have a greater impact on the atrial depolarization dynamics and, through the atrioventricular node, on the ventricular one. The identification of the most sensitive parameters would not only increase our comprehension of the electrophysiology phenomena, but it would also allow to improve existing computational models. Furthermore, determining what parameters influence the initial cardiac activation through sensitive analysis, as done here, is a first step towards reduced order models and the design of effective inverse calibration for patient-specific applications.

The paper is organized as follows. The computational model for the fast conduction atrial bundles based on the monodomain equations coupled with the ten Tusscher–Panfilov cellular model is detailed in (Sect. 2.1). The uncertainty PDFs of the input parameter space owing to the variability among individuals is calibrated in Sect. 2.2

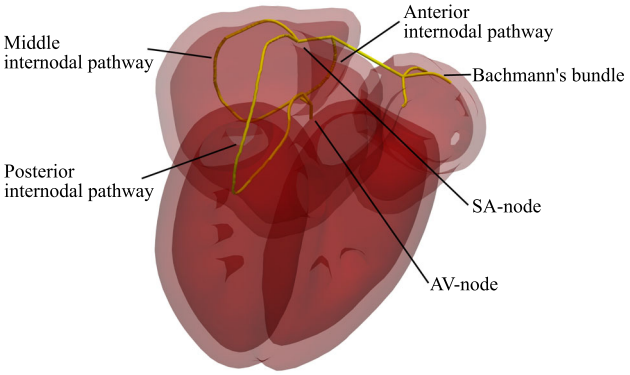

Fig. 2 Computational domain of the atrial fast conduction network (yellow) and the surrounding myocardium (red)

using available experimental data from the literature, while the QoIs of the study are defined in Sect. 2.3. The UQ analysis is based on a metamodelling technique (polynomial chaos expansion [10,11]) with a quasi Monte Carlo Sobol' low discrepancy sampling strategy so that to minimize the size of the dataset. The metamodel performance in reproducing the QoIs as obtained by the full electrophysiology model is verified through a cross validation strategy and the confidence intervals of the sensitivity indices are calculated using the bootstrap method as detailed in Sect. 3. Section Sect. 4.1 reports the sensitivity analysis of the selected QoIs on the input parameter space using the Sobol' sensitivity index, whereas the corresponding forward analysis, still obtained by the PCE, is reported in Sect. 4.2. A final discussion of the UQ results and future developments of the work are proposed in Sect. 5.

2 Electrophysiology problem, input parameter and quantities of interest

2.1 Bidomain/monodomain equations for the fast conductive bundles

The computational domain consists of four bundles, with three of them (the posterior internodal pathway, the middle internodal pathway, the anterior internodal pathway) originating from the SA-node, while the fourth one, the Bachmann's bundle, connects the right and left atrium among them and bifurcated into three small bundles within the left atrium, see Fig. 2.

The bundles are immersed in the atrial endocardium through some control points and, consequently, any modification of the atrial geometry studied in the UQ analysis (e.g. owing to a different volume of the cardiac chambers) directly affects the bundles geometry, which move so that to follow the location of the atrial control points. For any configuration of the atrial network, the bundles are automatically re-meshed in order to have the same spatial discretization for all UQ samples, see Appendix 1 for more details about the convergence of the numerical method.

The propagation of the electrical front through the myocardium is governed by the bidomain equations where the conductive tissue is modelled as an interior and exterior media [3]. Owing to the slenderness of the fast conduction bundles they can be considered as a network of one dimensional fibers that bifurcate and intersect at the network nodes and, as a consequence, the bidomain equations are equivalent to the monodomain equations as the intracellular and extracellular electrical conductivities reduce to scalar quantities necessarily proportional one each other:

$$\begin{aligned} C_m \frac{\partial v}{\partial t} + I_{ion}(v,\xi) + I_s &= \chi^{-1} \frac{\partial}{\partial s}\left(M \frac{\partial v}{\partial s}\right), \\ \frac{\partial \xi}{\partial t} &= F(v,\xi). \end{aligned} \tag{1}$$

Here v is the unknown transmembrane potential, $\chi = 140\ \mathrm{mm}^{-1}$ and $C_m = 0.01\,\mu\mathrm{F\,mm}^{-2}$ are the surface-to-volume ratio and the membrane capacitance of the cells [12]. The effective conductivity M is assumed to be uniform over the computational domain and is equal to half the harmonic mean of the intracellular and extracellular conductivities $M = \frac{M_{int} M_{ext}}{M_{int}+M_{ext}}$. The quantity I_{ion} is the net ionic current across the cell membrane and it is determined using the the ten Tusscher–Panfilov cellular model [13], which is indicated in compact form in the second Eq. (1). The solver imposes homogeneous Neumann boundary conditions on the transmembrane potential, whereas the network nodes are automatically handled by the FEM library as internal dofs and branching conditions do not need to be imposed. For each tissue location, the cellular model is given by a set of nonlinear ordinary differential equations (19 in our case that are not reported here for the sake of brevity) that is two-way coupled to the monodomain equation through the cell model state vector ξ and the transmembrane potential v. The current I_s corresponds to the electrical stimulus applied at SA-node location (see Fig. 3) where the electrical propagation originates:

$$I_s = S_a(\mathcal{H}[t] - \mathcal{H}[t - S_d]), \tag{2}$$

with S_a and S_d being the stimulus amplitude and duration, t the time within a heart beat and $\mathcal{H}[\cdot]$ the Heaviside function.

The governing Eq. (1) are discretized on a one-dimensional domain immersed in the atrial endocardium using the electrophysiology library cbcbeat [14], which is based on the finite element library FEniCS [15]. The monodomain Eq. (1) is integrated in time using a fractional step method based on the Crank-Nicholson scheme and the cellular model is solved

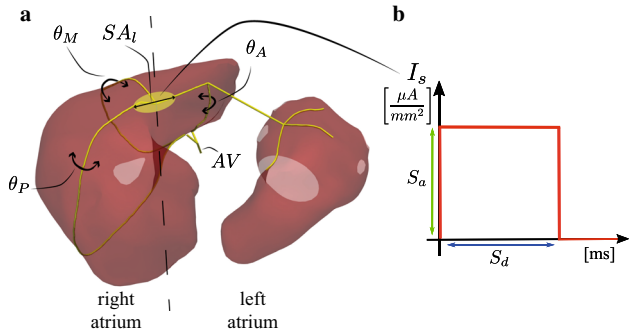

Fig. 3 **a** Atrial electrical pathways with sketched the angle parameters θ_A, θ_M, and θ_P along with the size of the sinoatrial node SA_L. **b** Stimulus current as a function of time, the parameters S_a and S_d indicate the amplitude and duration of the stimulus

in each mesh cell using a Rush-Larsen integration scheme, see Refs. [9,16]. The resulting average CPU time cost to solve a complete activation of the fast conduction bundles until reaching the AV-node on a reference grid of 2397 linear elements (corresponding to 47940 degrees of freedom including the ones of the cell model) and using a time step of $\mathrm{d}t = 5 \times 10^{-3}$ ms is of about 30 CPU-minutes (defined as the time it takes to run the program on a 1 GHz reference processor). The computational resources used for the analysis comprise an Intel Xeon Processors with 16 cores (E5-2620 v3 - 15M Cache, 2.40 GHz) that allow to run the same number of simulations simultaneously.

2.2 Input parameters

In order to run a global sensitivity analysis of the fast bundles electrical activation on the model input parameters, their uncertainty PDFs have to be determined from the in-vitro an in-vivo data reported in the literature. Unfortunately, these input PDFs are usually not available and even when systematic measurements of clinical quantities on a large population are carried out (e.g. the volume of the heart chambers) only the first (the mean μ) or the first and second (the mean μ and standard deviation σ) statistical moments of the PDF are reported in the literature. In such cases, in information theory, the PDF shape matching the statistical moments available is typically selected as the one maximizing the Shannon entropy (or its continuous extension) [17] as done here. In particular, in the case the PDF is known to be bounded in the interval $[a, b]$, the corresponding PDF maximizing the entropy is the uniform random variable $\mathcal{U}[a, b]$. On the other hand, if also the experimental mean value μ and standard deviation σ are available, a truncated normal distribution $\mathcal{N}_{[a,b]}(\mu_T, \sigma_T)$ should be considered. With formalism $\mathcal{N}_{[a,b]}(\mu_T, \sigma_T)$ we indicate the truncated normal distribution with mean $\mu_T = \mu$ and variance $\sigma_T = \sigma$, which is the maximum entropy distribution for fixed mean, variance and support.

The left atrium volume can be measured using several non-invasive techniques such echocardiography and magnetic resonance imaging (MRI) and a significant statistical difference between male and female atrial size is observed whereas the patient age weakly influences the atrial volume change for healthy subjects [18].

The mean and standard deviation of the left atrial volume measured on a population of 45 females and 63 males is equal to (41, 11) ml and (46, 14) ml, respectively. These results were obtained throughout a CMR (cardiovascular magnetic resonance imaging) procedure [19], with lower and upper bounds of (20, 120) ml measured on a larger population using MRI (including both genders) [20]. It should be noted that although both CMR and echocardiography can provide high resolution data, the volume chamber is typically evaluated by a human operator that necessarily introduces an additional source of uncertainty [19]. It is not possible, however, to distinguish the impact of the human operator on the measure of the volume chamber and the variability of this geometrical parameter is here ascribed to the individual variability only.

According to the principle of maximum entropy mentioned above, the left ventricle volume for males (V_m) and females (V_f) is modelled as two random variables distributed according to the truncated Gaussian distributions $\mathcal{N}_{[20\mathrm{ml},120\mathrm{ml}]}(\mu_T = 46\ \mathrm{ml}, \sigma_T = 14\ \mathrm{ml})$ and $\mathcal{N}_{[20\mathrm{ml},120\mathrm{ml}]}$ $(\mu_T = 41\ \mathrm{ml}, \sigma_T = 11\ \mathrm{ml})$.

In the UQ analysis, left and right atrial volume are assumed to be correlated and the same random variable (V_m for male and V_f for female population) is used to vary the volume of both chambers. The one-dimensional bundle geometry lies within the atrial myocardium with a nominal orientation of bundles as reported in Fig. 3a. The internodal angles are varied over their nominal orientation by an angular rotation around the vertical axis passing by the SA-node (dashed line) of size θ_A for the anterior, θ_M for the middle (Wenckebach) and θ_P for the posterior (Thorel) bundle, which are modeled as uniform distributions with amplitude $\pm\,\pi\,/7$ so that to vary significantly the bundles orientation but avoiding to overlaps and cross intersections among them.

Regarding the electrical properties of the fast conduction network, the input parameter space includes the electrical conductivity M influencing the conduction velocity of the fibers (see the monodomain Eq. (1)). The uncertainty PDF of the electrical conductivity is obtained in a reversed engineering fashion from the conduction velocity that is indicated to be of about 1–1.1 m/s [1,21] and in general below 2 m/s [2]. Hence, we have considered the conduction velocity to be bounded within the interval 1–2 m/s (in agreement with the velocity range measured in the canine atrial pathways, 0.88–1.66 m/s [22]), which corresponds to an electrical conductivity range of $M = 0.33 - 1.41$ S/mm according to the deterministic relation between the conduction velocity and electrical conductivity reported in Appendix 1. As only the

Table 1 Input parameters for the sensitivity analysis

Variable	Symbol	Nominal value	Distribution
Volume males	V_m	46 ml	$\mathcal{N}_{[20,120]}(\mu_T = 46, \sigma_T = 14)$
Volume females	V_f	41 ml	$\mathcal{N}_{[20,120]}(\mu_T = 41, \sigma_T = 11)$
Anterior internodal	θ_A	0	$\mathcal{U}[-\pi/7, \pi/7]$
Middle internodal	θ_M	0	$\mathcal{U}[-\pi/7, \pi/7]$
Posterior internodal	θ_P	0	$\mathcal{U}[-\pi/7, \pi/7]$
Electrical conduction	M	0.87 mS/mm	$\mathcal{U}[0.33, 1.41]$
SA stimulus duration	S_d	2.5 ms	$\mathcal{U}[0.5, 5.5]$
SA stimulus amplitude	S_a	1 mA/mm^2	$\mathcal{U}[0.5, 1.5]$
SA size	SA_l	6.85 mm	$\mathcal{U}[5.2, 8.5]$
Extra AV time	AV_d	90 ms	$\mathcal{U}[80, 100]$
Maximal I_{Na} Conductance	G_{Na}	14.838 nS/pF	$\mathcal{U}[11.870, 17.805]$
Extracellular Na Concentration	Na_O	140 mM	$\mathcal{U}[112, 168]$
Extracellular K Concentration	K_O	5.4 mM	$\mathcal{U}[4.32, 6.48]$

The bounds, mean and standard deviation of the PDFs reported in the last column have the same physical dimensions of the corresponding nominal value

mean value and the bounds for the electrical conductivity are known, a uniform distribution is considered as reported in Table 1.

Furthermore, the sensitivity of the bundles electrical activation on the duration S_d and amplitude S_a of the stimulus in the SA-node, along with extension of the SA is studied. The input current stimulus, see Fig. 3a, is modelled as a rectangular function with duration and amplitude equal to S_d and S_a whose uncertainty is modeled as uniform distributions containing the values used in the literature to activate the wavefront propagation [23]. On the other hand, the length of the SA is known to vary between 5.2 and 8.5 mm [24], and these values have been used as bounds for the spatial extension of the stimulus applied in the SA-node. Additionally, the variability of the time delay in the propagation of the electrical signal occurring the AV-node, AV_d, is considered as a uniform PDF with mean value 90 ms and bounds equal to ± 10 the mean value [1].

The effect of the input parameters of the ten Tusscher–Panfilov cellular model on the electrical activation is studied by accounting for variability of the maximal I_{Na} conductance, G_{Na}, of the extracellular Na concentration, Na_O, and of the extracellular K concentration, K_O, that were seen to be the most relevant parameters in previous analyses [9,25]. A uniform uncertainty of $\pm 20\%$ the nominal value around the nominal value itself is considered.

The dimension of the input parameter space is thus equal to $d = 12$ and the corresponding PDFs are reported in Table 1. As the relationships between these input random variables are unknown, they are modeled as independent random variables.

2.3 Quantities of interest

As the main objective of the analysis is to investigate the effect of the model input parameters introduced above on the propagation of the electrical wavefront through the atrial pathways, the quantities of interest (QoIs) of the UQ analysis are defined as the activation times of the network nodes. Referring to Fig. 4, the UQ analysis monitors the time needed to reach the two junctions of the AV-node (t_1, t_2), along with the activation times of the tips of the Bachmann's bundle (t_3, t_4, t_5). Additionally, two further QoIs are defined as the activation time of the upstream $t^* = \min(t_1, t_2)$ and downstream t_{AV} tip of the AV. We recall that the downstream tip of the AV-node transmits the electrical propagation front to the ventricular fast conduction system (not included in this UQ analysis). A last QoI is given by the conduction velocity v_c of the propagation of the depolarization front, which is uniform across the bundles since the electrical conductivity and the cell model properties are uniform in the domain. Without loss of generality the conduction velocity is thus measured at the middle internodal pathway.

3 UQ methods

3.1 Polynomial chaos expansion

The sensitivity of the QoIs on the input parameters is investigated through a variance-based global sensitivity analysis using first (also called importance measures) and total order Sobol' indices [26]. These quantities are defined as the influence of input parameters on the variance of the QoIs and are able to describe the combined effects of multiple input

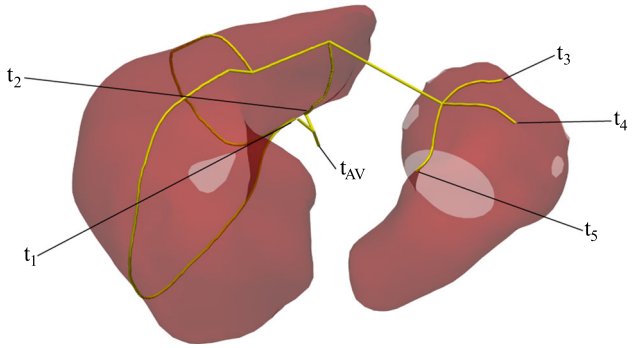

Fig. 4 Activation time at the AV bundle (t_1, t_2), at the end of the Bachmann's bundle (t_3, t_4, t_5) and at the downstream tip of the AV-node t_{AV}

variables, thus providing a deeper understanding of the physical system at study. Computing the Sobol' indices using a direct approach can be computationally expensive because the QoIs dependence on the input variables is obtained by solving the full system (the monodomain model here). As an example, given d input parameters, the computational cost for evaluating the first order Sobol' indices is $\mathcal{O}(dN^2)$ using a a standard Monte Carlo (MC) approach or $\mathcal{O}((d+2)N)$ applying the Saltelli's algorithm, with $N \approx 10^3$ the size of the samples needed to approximate one of the input variables. In order to reduce the computational cost of the UQ analysis, a polynomial chaos expansion (PCE) approach is adopted [11], which belongs to the family of the metamodelling techniques where the sensitivity indices are evaluated using a simplified model rather than the whole physical system as done in the direct methods. The adaptive procedure for the PCE calibration used here has been previously validated in the case of the electrical depolarization of the ventricular myocardium [9]. All of the details of the algorithms, the validations and the convergence checks can be found in the above reference; only the main features are summarized here. The metamodel is built so that to reproduce/approximate the input–output relation of the governing equations using a training and a testing dataset.

In particular, given a computational model, $G : \mathcal{D}_X \subset \mathbb{R}^d \to \mathbb{R}$, the uncertainty of the input parameters is modeled by a random vector X prescribed by joint probability density function $f_X(x)$ [27] and the QoI $Y = G(X)$ is obtained by propagating the uncertainty on X through G. Assuming that the input variables are statistically independent, the joint PDF is the product of the d marginal distributions $f_X(x) = \prod_{i=1}^{d} f_{X_i}(x_i)$ for each $\mathcal{D}_{X_i}$ and we can define the inner product for each single variable X_i and for any two functions $\phi_1, \phi_2 : \mathcal{D}_{X_i} \to \mathbb{R}$ as: $\langle \phi_1, \phi_2 \rangle := \int_{D_{X_i}} \phi_1(x)\phi_2(x) f_{X_i}(x)\mathrm{d}x$ and use it to define an orthonormal family of polynomials $\{P_k^{(i)}, k \in \mathbb{N}\}$. This set of univariate orthonormal polynomials can be used to define a family of multivariate ones. In fact, given a multi-index $\alpha = (\alpha_1, \cdots, \alpha_d), \alpha_i \in \mathbb{N}$, the associated multivariate polynomial can be defined as $\Psi_\alpha(x) := \prod_{i=1}^{d} P_{\alpha_i}^{(i)}(x_i)$. The set of all multivariate polynomials in the input random vector X forms a basis of the Hilbert space , in which $Y = G(X)$ is given by the so called polynomial chaos expansion:

$$Y = \sum_{\alpha \in \mathbb{N}^d} y_\alpha \Psi_\alpha(X). \tag{3}$$

This infinite series has to be truncated in order to get a finite one approximating $Y = G(X)$ and different truncation strategies are possible depending (i) on how to enumerate the element of the multivariate basis and (ii) on how many terms of the basis have to be retained. The standard (linear) enumeration strategy is based on the total degree of a multivariate polynomial Ψ_α (with $\|\Psi_\alpha\| := \sum_{i=1}^{d} \alpha_i$) and is defined as the lexicographical order with a constraint of increasing total degree (e.g. for a two dimensional multi-index $(0,0) < (0,1) < (1,0) < (2,0) < (1,1,) < \cdots$). The chosen selection strategy is a fixed one, in which the total degree p is fixed and all the coefficients with total degree smaller or equal to p are retained. It should be noted that a linear enumeration coupled with a fixed truncation rule corresponds to a dimension of the basis with cardinality $\binom{d+p}{p}$, with p the polynomial degree and d the size of the input space [27]. The optimal hyper-parameter for each metamodel (i.e. the total degree) is calculated using an adaptive strategy [9].

The PCE coefficients are chosen using a least squares strategy (LQS hereafter), which minimizes the least squares error of the metamodel response on the training set. The main advantage of using an LQS is the fact that the training dataset can be extended if needed, whereas the use of integration rules based on Gaussian point can not. A training dataset of 2000 samples is here built using a quasi Monte Carlo method (QMC) with low discrepancy Sobol' sequence in order to maximize the information contained and avoid clustering phenomena within the dataset [26]. The QMC has, indeed, a faster asymptotic converge rate for low number of parameters, $\mathcal{O}\left(\frac{\log(N)^d}{N}\right)$ where d is the input dimension, compared to the standard MC, $\mathcal{O}\left(\frac{1}{\sqrt{N}}\right)$ [28].

3.2 Metamodel validation and confidence intervals

Metamodelling techniques require a validation protocol to verify their ability to reproduce the results of the original physical system. In this analysis the risk of underfitting and overfitting is measured by evaluating the coefficients R^2 and Q^2. Given the training (testing) dataset of size n, described by the couples $(\mathbf{x}_i, y_i)_{i=1}^n$ with y_i the QoIs corresponding to the set of input $\mathbf{x}_i$, and the prediction of the metamodel f for the same input dataset $(\mathbf{x}_i, \hat{y}_i := f(\mathbf{x}_i))_{i=1}^n$, the coefficient

of determination is defined as $R^2(Q^2) := 1 - \frac{SS_r}{SS_t}$, where $SS_r := \sum_{i=1}^{n}(y_i - \hat{y}_i)^2$ is the residual sum square normalized for the total sum of squares $SS_t := \sum_{i=1}^{n}(y_i - \overline{y})^2$ with $\overline{y} = \frac{1}{n}\sum_{i=1}^{n} y_i$. The R^2 index is commonly used in regression analysis to measure the metamodel performance in reproducing the variability within the training dataset with values close to one implying that the metamodel is well-trained, whereas low Q^2 and a high R^2 would correspond to an overfitting condition [29].

In contrast with a direct approach such as Saltelli's algorithm , the confidence intervals for Sobol' indices can not be derived from the asymptotic distribution of the estimators of the indices, but they can still be assessed without performing further simulations through a resampling method, the bootstrap [30]. The main idea is to create a few artificial datasets of different sizes by sampling with replacements the individual elements of the original training one. These artificial datasets are then used to calculate the Sobol' indices (using the PCE method introduced above), thus obtaining an empirical distribution of the indices quantifying the stability of the results with respect to a variation of the input dataset. The α-percentile bootstrap interval is defined as: $[S_{i[\alpha/2]}, S_{i[1-\alpha/2]}]$ where $S_{i[\alpha/2]}$ and $S_{i[1-\alpha/2]}$ are the $\alpha/2$ and the $1-\alpha/2$ empirical quantiles of the ith Sobol' index distribution [31]. This interval does not require hypotheses about the S_i distributions (compared to standard intervals which assume normality [31]) but it needs many resamplings to estimate them accurately.

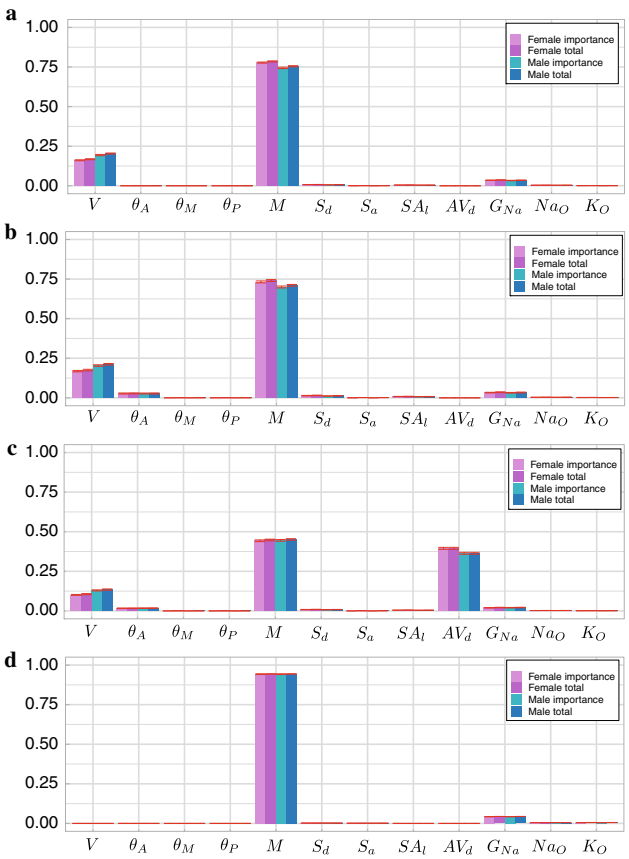

Fig. 5 Importance measures (e.g. female/male importance) and Sobol' total order indices (female/male total) for **a** t_4, **b** t^*, **c** t_{AV} and **d** v_c. Females (males) population is indicated by the pink (blue) histograms, whereas the errorbars indicate the confidence intervals of the metamodels

4 Results

4.1 Sensitivity analysis

An optimal PCE is trained and validated as detailed in the previous section for each QoI and the resulting hyper-parameters are summarized in Table 2. Although the resulting total polynomial degree is relatively low (equal to to 3) for each QoI the metamodels are able to describe over 99% the output variance, as visible by the R^2 coefficients reported in Table 2. Furthermore, the non-zero coefficients of the PCEs, are related to the interactions of single variables, which implies that the PCEs neglect high order interactions (i.e. associated with a polynomial with high degree in more than one variable [32]) and that the Sobol' total order are expected to be similar to the corresponding importance measure. The cost of producing the entire dataset for the metamodel approach is approximately 42 CPU-days, where a CPU-day is defined as a compute day run on a 1 GHz reference processor, while the metamodel is trained in about 1 CPU-minute.

As the input uncertainty of the atrial volume is different for male and female population, see (Sect. 2.2), two different sensitivity analyses are carried out for each QoI that are depicted by the blue and pink histograms in Fig. 5. The small error bars on top of the histograms (corresponding the 95%-confidence interval computed using the bootstrap method with 500 resamplings) indicate that the training dataset is sufficiently large to accurately evaluate the Sobol' indices, see Appendix 1 for a convergence analysis of the PCE method. We anticipate that, as the sensitivity results of t_1, t_2 (t_3, t_5) are similar to the ones of t^* (t_4) their Sobol' indices are not reported in the figure.

As visible in Fig. 5a, b both t^* and t_4 are sensitive on the electrical conductivity (with an importance of about 80%) and on the size of the atrial chambers (with a lower importance of about 20%). The sensitivities presented in Fig. 5 are described in terms of both first order Sobol' indices (importance measure, defined for females and males as female importance and male importance) and total order (defined for females and males as female total and male total). Additionally, the cell model parameter G_{Na} has a minor effect (with about 5%) importance, whereas the rest of the input parameter space, including the duration and amplitude of the

Table 2 Optimal metamodels selected by the adaptive PCE methodology

QoI	enumeration strategy	truncation strategy	p	PCE cardinality	R^2/Q^2
Female t_4	Linear	Fixed degree	3	364	0.991/0.986
Female t_4	Linear	Fixed degree	3	364	0.999/0.998
Male t^*	Linear	Fixed degree	3	364	0.992/0.987
Male t^*	Linear	Fixed degree	3	364	0.999/0.999
Female t_{AV}	Linear	Fixed degree	3	455	0.995/0.990
Male t_{AV}	Linear	Fixed degree	3	455	0.995/0.990
v_c	Linear	Fixed degree	2	78	0.999/0.999

electrical stimulus along with the length of the SA-node, have a negligible effect on the QoI. A similar weak influence on the QoIs is observed for the angle perturbation of the bundles with the only exception of θ_A that slightly influences t^* because the anterior internodal pathway is the shortest path connecting the SA-node to the AV-node and a variation of its length owing to the angular variation (we recall that the bundle is constraint on the atrial endocardium) affect the time at which the AV-node is reached by the electrical propagation front. Importantly, males and females population manifest similar sensitivities of t_4 and t^* on the input parameters with a relatively larger sensitivity of the female population on the electrical conductivity and a relatively smaller one on the atrial volume.

Conversely, the activation time of the lower tip of the AV-node (the one towards the ventricular network), t_{AV}, is not only sensitive to the electrical conductivity (importance of about 45%) but is also affected by the time delay occurring in the AV-node AV_d (importance of about 35%–45%). It should be noted that even the small percentage variation of the AV_d considered here (about $\pm 11\%$ of the mean value, see Table 1) has a relevant effect on t_{AV} and a larger variation of AV_d would further increase the time needed to fully activate the AV-node. Furthermore, the AV_d is slightly more important in female hearts with respect to the male population (one tailed t-test with $N = 500$ refusing the hypothesis that male AV_d is lower the female AV_d at a level $\alpha = 10^{-3}$ for both importance measure and total order) as the volume variation for females has a lower standard variation (11 ml against 14 ml for males), thus naturally increasing the sensitivity of the other parameters. Regarding the other parameters, the t_{AV} is seen to also depend on the atrial volume, on G_{Na} and on θ_A, whereas the other angular perturbations and the current stimulus parameters (S_a, S_d and S_l) have a negligible effect on the QoI.

As expected in diffusion dominated problems, the conduction velocity v_c is greatly sensitive on the electrical conductivity M with an importance exceeding 90 %, see Fig. 5d. The complementary part of the importance indices is shared among the three input parameters of the cell model with a major influence of G_{Na}. This result differs from what observed in the two-dimensional solution of the bidomain equations where the Na_O and K_O were seen to influence the ventricular activation time more than G_{Na} [9].

4.2 Forward analysis

Let now turn to evaluate the PDFs of the QoIs through a direct UQ strategy using the trained metamodel (see Table 2), rather than the full monodomain system. The metamodels, one for each QoI, are applied on a very large input dataset (10^6 samples) sampled using a Latin hypercube strategy to avoid clustering phenomena, and the corresponding output dataset is used to approximate the PDFs of the QoIs that are reported in Fig. 6. The computational cost of this forward analysis using the metamodel trained for the sensitivity analysis is negligible (of the order of CPU-minutes), whereas the same forward direct analysis would have required 57 CPU-years using the initial electrophysiology Eq. (1).

The PDFs of the activation times t^* and t_4 have a similar skewness and kurtosis for both, male and female population but with a larger mean value, respectively of 6.4% and 5.8%, for the former, see Table 3. On average, t^* corresponds to what observed in-vivo (about 30 ms [1]), even if the high standard deviations resulting from our forward analysis implies that it is not uncommon to have longer activation times. According to the PDFs, the probability of a normal/physiological activation time of the AV-node corresponding to a t^* comprises between 20 and 50 ms is equal to 97.6% for females and 96.3% for males, where in both cases the positive skewness of the PDFs favors longer activation time with respect to the mean t^* rather than shorter ones. Specifically, the probability of experiencing an AV activation time shorter than 10 ms is about 0, whereas a t^* shorter than 20 ms has a probability to occur of 0.7% and 0.5% for females and males, respectively. On the other hand, the probability of having an AV activation time greater than 50 ms is

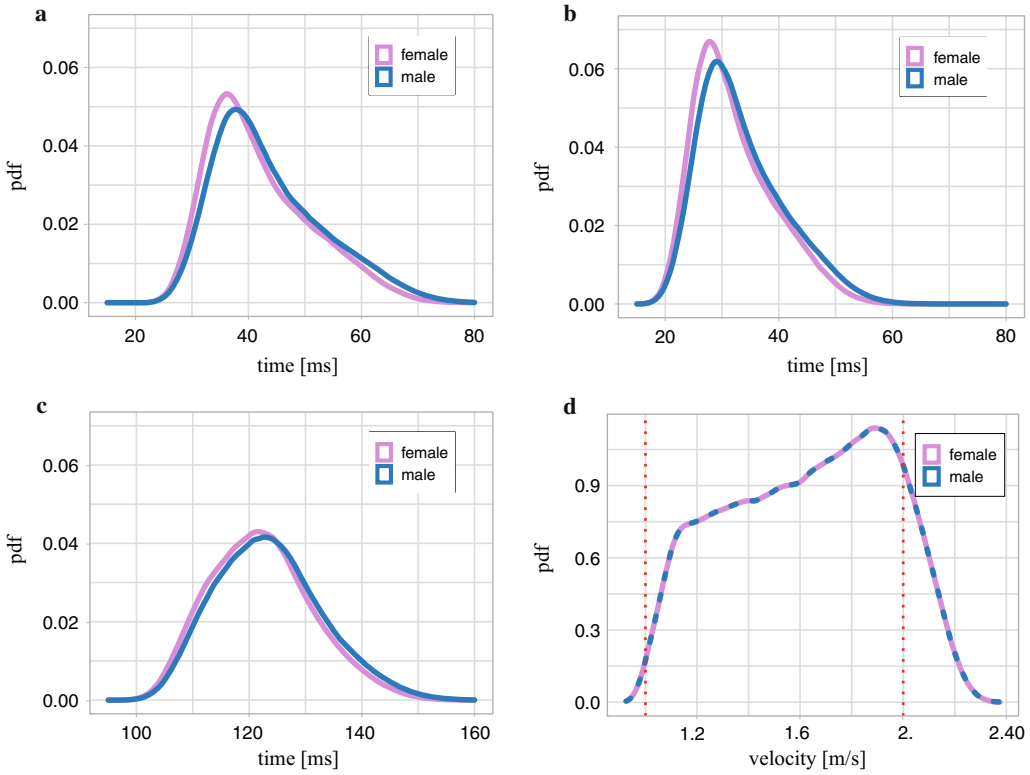

Fig. 6 PDF of the QoIs obtained using 10^6 samples evaluated through the optimal metamodel: **a** t_4, **b** t^*, **c** t_{AV} and **d** v_c

Table 3 Statistical moments for t^*, t_4, t_{AV} and v_c

	Female t^*	Female t_4	Female t_{AV}	Male t^*	Male t_4	Male t_{AV}	v_c
Mean	32.19	41.2	122.19	33.55	43.62	123.54	1.62
Std	7.13	9.12	9.15	7.62	9.72	9.54	0.31
Skewness	0.74	0.73	0.34	0.73	0.73	0.37	−0.14
Kurtosis	3.13	3.00	2.85	3.16	3.05	2.90	1.96

The means and standard deviations of the times are expressed in ms, the velocity in m/s

larger for the males population (3.2% probability) than for females (1.6% probability).

The PDF of the activation time at the downstream tip of the AV-node t_{AV}, is shown in Fig. 6c, while the statistical moments are reported in Table 3. As could be inferred from the Sobol' indices, the sensitivity of t_{AV} on the time delay in the AV, AV_d, reduces the differences between the PDFs of males and females with relative difference of the mean values of about 1.1%. Furthermore, the statistical dispersion for t_{AV} (evaluated by variation coefficient σ/μ), is also reduced (−7.4% for females and −7.7% for males) with respect to the one observed in t^* (−22.1% and −22.7 %) The PDF for the t_{AV} results in line with the medical knowledge, with an about null probability of activation time higher than 150 ms that would compromise a timely ventricular contraction. [1].

As it could have been anticipated by noting that the Sobol' index corresponding to the volume parameter is about null, no differences are present among the PDFs of the v_c for the males and females population shown in Fig. 6d. Moreover, the PDF skewness is a consequence of the nonlinear relation between the conduction velocity and the electrical conductivity documented in Appendix 1. Specifically, as a symmetric PDF around its mean has been considered to model the uncertainty of the electrical conduction, the probability of v_c to be slower (faster) than the physiological lower (upper) bound of 1 m/s (2 m/s) is below 0.5% (13%).

5 Discussion and future developments

In this work, we have investigated the global sensitivity analysis of the electrical activation of the atrial fast conduction network on the geometrical and electrical input parameters of the electrophysiology model. The network has been modelled as four mono-dimensional bundles, with three of them connecting the SA-node to the AV-node whereas the last one joins the right with the left atrium. The propagation of the electrical depolarization front through the myocardium is governed by the bidomain equations, which, in the case of a one-dimensional domain, are equivalent to the monodomain model. The uncertainty PDFs of these input parameters have been taken from the experimental data available and the gender difference has been accounted for in the UQ analysis by considering two different PDFs for the atrial volume of the females and males population. Moreover, the PDF of the electrical conduction has been obtained through an inverse calibration of the conduction velocity data from the literature. The UQ analysis is based on the PCE method with a different metamodel trained for each QoI on a training dataset, which is built running the full monodomain model. The risk of overfitting has been assessed by testing the metamodels performances against a testing dataset, which is independent of the training one, whereas the confidence intervals of the Sobol' indices, computed using the bootstrap technique, indicate that the sensitivity results are converged with respect to the size of the dataset used to train the metamodel.

For both the female and male population, the activation times of the atrial fast conduction network, t_4, t^* and t_{AV}, are seen to be sensitive to the electrical conductivity M, the atrial volume V and the temporal delay in the AV AV_d with a total effect on their variance exceeding 95 %. Importantly, the relative positions of the internodal pathways that, to the authors' knowledge, can be hardly measured in-vivo and are not sufficiently documented in the literature only play a marginal role in the activation of the atrioventricular node according to the Sobol' indices (total effect on the QoI variance below 5%). According to our results, these geometrical input parameters could be disregarded in future UQ analyses. The smaller atrial volume (on average) of the female population leads to a reduced effect of this input parameter on the variance of the QoIs compared to the males population, in particular the Sobol' total order of V reduces from 0.21 to 0.17 for t^* and from 0.20 to 0.16 for t_4 . Consequently, the other inputs have a larger effects on the QoIs in the female population, as an example, the sensitivity of t^* (t_4) on M and G_{Na} increases from 0.71 and 0.034 (0.75 and 0.0351) in the male population to 0.74 and 0.035 (0.78 and 0.0354) in female one.

On the other hand, the conduction velocity is only sensitive to the electrical conduction (with an effect of about 95%) and to the maximal I_{Na} conductance (G_{Na}, with an effect of about 5%) while the other ten input parameters, including the extracellular Na concentration, Na_O, and the extracellular K concentration, K_O, have a negligible effect on the QoIs variance. This result differs from what observed in the solution of the bidomain equations in a multi-dimensional domain where both the extracellular Na concentration, Na_O, and the extracellular K concentration, K_O, were seen to have a greater effect on v_c with respect to G_{Na} [9,33]. As a consequence, isolating the internodal pathways from the surrounding three-dimensional myocardium yields to a smaller input parameter space and, consequently, to a reduced computational cost for future UQ studies.

It should be noted that both the electrical activation of the network and the conduction velocity are insensitive to the parameters of the electrical stimulation (stimulus intensity S_d, stimulus amplitude S_a and size of the SA-node SA_l) and any simulation protocol able to originate the depolarization front is suitable in such electrophysiology models. Further studies, however, could assess the possible differences in the electrical activation of the electrical pathways if the SA-node is modeled using a three-dimensional geometry integrated in the electrical network rather than as a localized in put current as done in this work [34,35].

The same metamodels used in the sensitivity analysis have been then used to determine the uncertainty PDF of the QoIs (forward UQ analysis) by producing a large dataset of 10^6 elements. The PDFs of the activation times are characterized by a positive skewness (i.e. with a longer right tail with respect to the left one) while the conduction velocity has a negative one. The PDFs of t_4 and t^* have a high statistical dispersion equal to $\sigma/\mu \approx 20\%$, while t_{AV} has a smaller dispersion (about 7.5%) owing to the higher sensitivity on the AV-delay, AV_d. The PDF of the activation times well agrees with the medical knowledge [1] with a probability for the AV-node to be reached by the electrical stimulus (t^*) in less than 20 ms or more than 50 ms below 0.7% and 3.2%, respectively (for both males and females population), while t_{AV} has an almost zero probability of being higher than 150 ms. We recall that the activation time of the ventricular tip of the AV-node t_{AV} plays a major role in the synchronization of atrial–ventricular contraction and if t_{AV} is not sufficiently long the ventricles would start contracting before the end of atrial systole, thus yielding to an inefficient blood pumping. Although the activation time of the whole atrial myocardium is known from the clinical evidence to have an average depolarization time of 148.8 ms with a standard deviation of 18.9 ms [36], these data can only be considered as an upper bound with respect to the activation time of the fast conduction bundles that is studied here. Indeed, the high conductivity structures should be fully activated before the surrounding myocardium depolarizes, which is in line with our UQ analysis where the average time needed for the electrical signal to reach the AV-node, t^*, results equal to 32.19 ms (33.55 ms)

for the females (males) population. Moreover, for both genders t^* is less than the lower bound of the activation time of the three–dimensional myocardium reported in the literature (defined as the mean value minus three times the standard deviation 148.8 ms $-$ 3 $\times$ 18.9 ms $=$ 92.1 ms) with a probability exceeding 99%.

The uncertainty PDFs of the conduction velocity v_c is seen to be skewed towards the high velocity range as it has been previously observed in the case of electrical conduction within the atrial myocardium by randomly perturbing both fibers orientation and local conductivities [37]. This result can be probably explained by the non-linear relationship between the electrical conductivity and the conduction velocity reported in Appendix 1, which means that considering a symmetric PDF of the electrical conductivity automatically introduces a skewness in the conduction velocity distribution and, eventually, in the PDFs of the other QoIs. Alternatively, considering a symmetric uncertainty PDF for the conduction velocity, it would greatly reduce the marked skewness phenomenon in the forward analysis, thus suggesting to use the conduction velocity as input parameter rather than the electric conduction. Nevertheless, proper calibration of the electric conduction could solve the problem of considering uniformly varied inputs with the consequent output asymmetry, and the model reduction carried out here offers a starting point for a Bayesian inverse calibration of the electrical conduction–conduction velocity from the available experimental measurements of the AV-activation time t^*. The sensitivity analysis, indeed, shows that the time needed for the depolarization front to reach the AV, t^*, basically only depends on M and V (with a reduced influence of G_{Na}) and all these quantities but M can be measured through non-invasive medical procedures such as MRI for the atrial volume [20] and ECG for t^* [36]). This is the optimal context for Bayesian inverse calibration where only an input parameter is unknown, which can be retrieved knowing the PDFs of the other physical quantities at play [38,39]. Similar techniques used in the framework of MICP (monodomain inverse conductivity problem) to calibrate space-dependent conductivity for two-dimensional [7] and three-dimensional [8] models can be adapted to the one-dimensional problem proposed here. Even the presence of local perturbations of conductivity can be taken into account both in the direct and inverse problem, possibly exploiting a multi-fidelity method applied using the monodomain as a high fidelity model and a simplified alternative (e.g. eikonal) as a low fidelity one [37].

A natural extension of the present UQ analysis would be to include the effect of the fast conduction bundles on the three-dimensional myocardial tissue surrounding them, thus allowing to investigate further QoIs commonly used in the medical field, such as the atrial activation time (that is expected to depend on the stimulus location [40]), the uniformity of the depolarization front propagation and the action potential duration [33,41], which are known to be relevant for the patient's health as they influence the efficiency of the atrial systole [1]. Given the proposed decomposition between the fast structures and the underlying three-dimensional fiber, the model to be used. The anisotropic and heterogeneous myocardium could also be modelled using the new fractional models [42,43], which show promising results in cardiac dynamics and can naturally integrate techniques for the calibration of the model parameters [44]. Furthermore, in addition to the healthy myocardium [45–48] the effect of pathologies can be included in the UQ analysis by accounting for modified electrical properties of the conductive medium [49–51]. As the electrical signal travels from the atria to the ventricles passing through the AV, this analysis could be also extended by adding the ventricular fast conduction bundles (including the Purkinje network) to investigate how sensitive is the ventricular activation to atrial dysfunctions such as atrial fibrillation [52]. A further open question calling for dedicated UQ studies, is the effect of the stimulation frequency on the action potential duration and the depolarization front propagation and, interestingly, the most relevant input parameters of the cellular model are expected to strongly depend on the stimulation frequency itself [53–55].

Acknowledgements This study has been performed with support of the 'Fluid dynamics of hearts at risk of failure: towards methods for the prediction of disease progressions' funded by the Italian Ministry of Education and University (Grant 2017A889FP).

Appendix A: Convergence of the electrophysiology model

The transmembrane potential averaged over the ventricular domain as a function of time is shown in Fig. 7. Each solid curve corresponds to a different simulation of the monodomain equations with the ten Tusscher–Panfilov model on a different grid with elements number varying from 600 to 4000 and different time step sizes [12]. The averaged transmembrane potential becomes basically grid independent for mesh resolution exceeding 2000 elements and, based on this result, a mesh with 2397 elements (corresponding to a $\Delta X = 0.25$ mm) and $\Delta t = 0.005$ ms is used for the UQ analysis. The corresponding computational cost to run a single simulation is of about 30 CPU-minutes and, consequently, the cost to build the UQ datasets is of about 42 CPU-days. The numerical simulation have been run on an Intel Xeon Processors (E5-2620 v3 - 15M Cache, 2.40 GHz), with 16 CPUs.

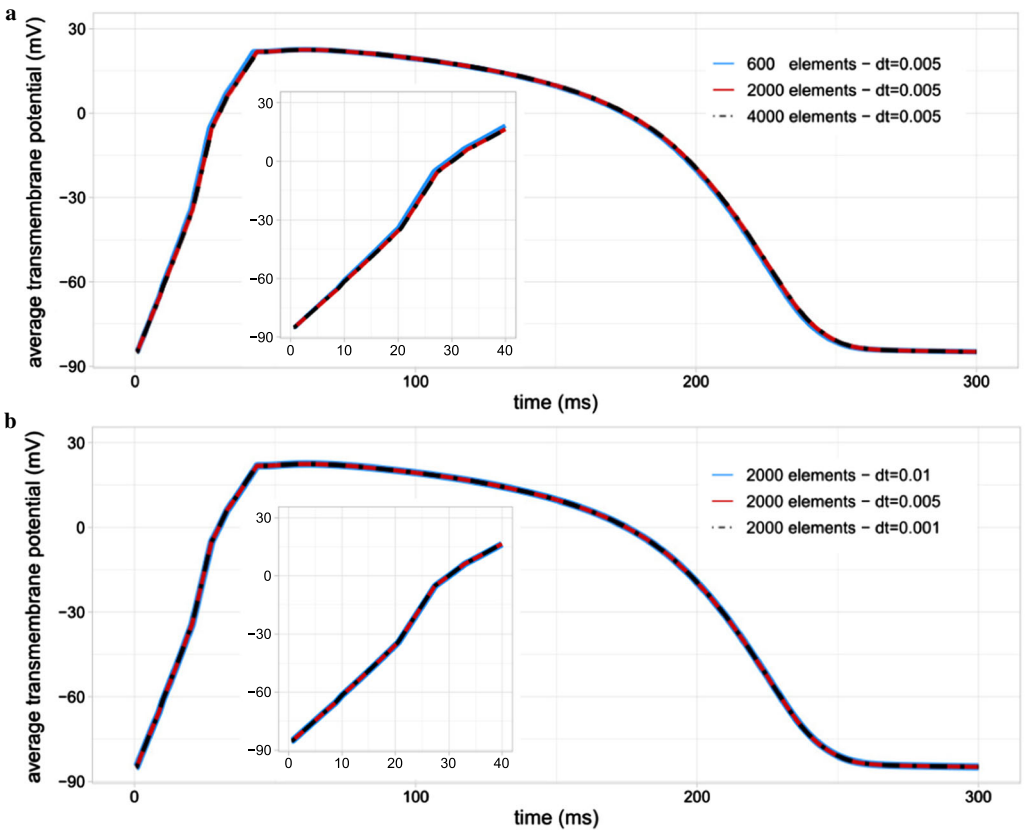

Fig. 7 Time behaviour of the average transmembrane potential in the atrial fast conduction network by refining **a** the spatial and **b** the temporal resolution. The insets show the same quantity within the initial fast depolarization phase

B: Convergence of the PCE analysis

Figure 8a shows the coefficient R^2 and Q^2 introduced in Sect. 2 for the case of t_{AV} in the female population as a function of the training dataset size. The optimal metamodel (see Table 2) is trained each time using a different training dataset with size ranging from 500 to 2000 and tested against the same testing dataset made of 200 samples. The R^2 index is stable with respect to the training data set size as the number of samples is larger than 500, which means that the variety of the metamodel is sufficient to describe the physical phenomenon at study. Conversely, lower size of the training dataset lead to a suboptimal value of the index Q^2, which corresponds to a reduced ability of the metamodel to predict values outside the training sample. Hence, the convergence of the difference R^2–Q^2 indicates that the metamodel can be considered stable when the size of the training metamodel exceeds 1000 cases. Similar results are obtained for the other QoIs and the males population (not reported here for the sake of brevity).

Another approach for testing the metamodel performance consists of evaluating its stability to a perturbation of the training dataset. Specifically, the results of the UQ analysis are shown as a function of the dataset size thus determining for what size they become stable, as shown in Fig. 8b where the Sobol' indices are seen to be stable for dataset size larger than 1000. The figure also reports the 5-percentile confidence intervals calculated using a bootstrap method on the training dataset.

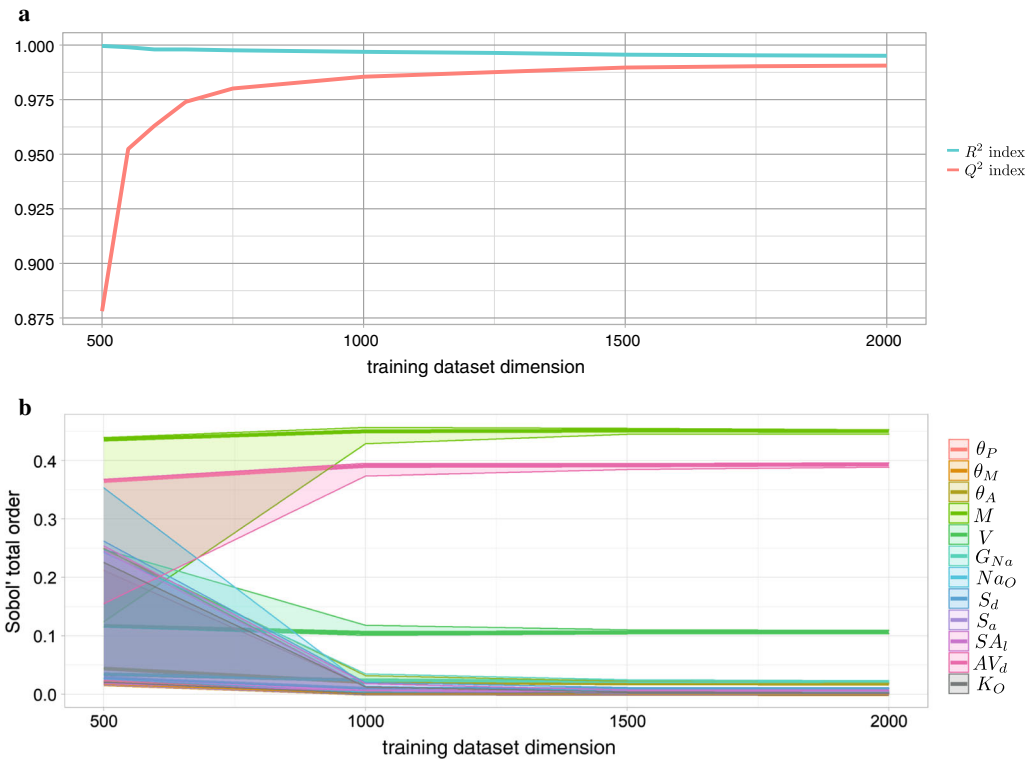

Fig. 8 **a** R^2 and Q^2 indices for t_{AV} of the female dataset. Indices are reported for an increasing size of the training dataset and a fixed testing dataset of size 200 is used to compute the corresponding Q^2 index. **b** Stability analysis of Sobol' indices for t_{AV} on the female dataset with 5-percentile confidence intervals calculated using a bootstrap methodology

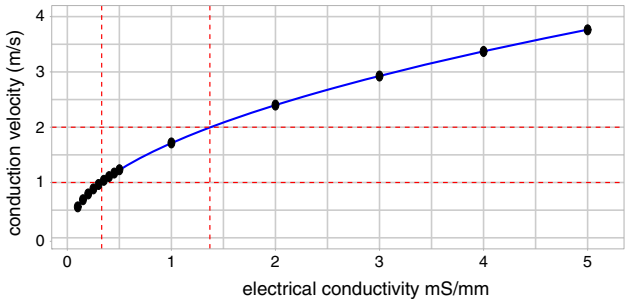

Fig. 9 Conduction velocity as a function of the electrical conductivity (black dots) with superimposed a square root interpolation function (blue line). The straight red lines indicate the ranges of the electrical conductivity and of the conduction velocity studied in the UQ analysis

C: Electrical conductivity vs conduction velocity

The electrical conductivity M is an important input parameter of the electrophysiology model. However, most of the available measurements in the literature refer to the conduction velocity rather than to the electrical conductivity [1,21,22]. For this reason, an inverse calibration has to be preformed to determine the electrical conductivities corresponding to the conduction velocities measured experimentally. In order to determine such relation between the electrical conductivity and the conduction velocity, the monodomain equations have been solved over a one-dimensional straight domain of length 100 mm for several electrical conductivity values. The corresponding conduction velocity is measured by selecting two points 50 mm apart each other inside the domain and monitoring their activation time (defined as the instant when the transmembrane potential exceeds -70 mV). The conduction velocity is thus measured as the ratio between the distance between the monitoring points and the time interval among their activation and is reported in Fig. 9 for spatial and temporal discretization of $\Delta x = 0.25$ mm and $\Delta t = 1 \cdot 10^{-3}$ ms and current stimulus applied at one tip of the domain as defined in equation (2) with S_d =2.5 ms, S_a =1 mA/mm^2 and $SA_l = 6.85$ mm.

References

1. Hall, J.E.: Guyton and Hall Textbook of Medical Physiology e-Book. Elsevier Health Sciences (2015)
2. Harrild, D.M., Henriquez, C.S.: A computer model of normal conduction in the human atria. Circ. Res. **87**, e25–e36 (2000)
3. Sundnes, J., Lines, G.T., Cai, X., et al.: Computing the Electrical Activity in the Heart, vol. 1. Springer, New York (2007)
4. Vigmond, E., Dos Santos, R.W., Prassl, A., et al.: Solvers for the cardiac bidomain equations. Progr. Biophys. Mol. Biol **96**, 3–18 (2008)

5. Sepulveda, N.G., Roth, B.J., Wikswo Jr., J.P.: Current injection into a two-dimensional anisotropic bidomain. Biophys. J. **55**, 987 (1989)
6. Pullan, A.J., Tomlinson, K.A., Hunter, P.J.: A finite element method for an eikonal equation model of myocardial excitation wavefront propagation. SIAM J. Appl. Math. **63**(1), 324–350 (2002)
7. Barone, A., Gizzi, A., Fenton, F., et al.: Experimental validation of a variational data assimilation procedure for estimating space-dependent cardiac conductivities. Comput. Methods Appl. Mech. Eng. **358**, 112615 (2020)
8. Barone, A., Carlino, M.G., Gizzi, A., et al.: Efficient estimation of cardiac conductivities: a proper generalized decomposition approach. J. Comput. Phys. **423**, 109810 (2020)
9. Del Corso, G., Verzicco, R., Viola, F.: Sensitivity analysis of an electrophysiology model for the left ventricle. J. R. Soc. Interface **17**(171), 20200532 (2020)
10. Eldred, M., Burkardt, J.: Comparison of non-intrusive polynomial chaos and stochastic collocation methods for uncertainty quantification. In: 47th AIAA Aerospace Sciences Meeting Including the New Horizons Forum and Aerospace Exposition, p. 976 (2009)
11. Sudret, B.: Global sensitivity analysis using polynomial chaos expansions. Reliab. Eng. Syst. Saf. **93**, 964–979 (2008)
12. Niederer, S.A., Kerfoot, E., Benson, A.P., et al.: Verification of cardiac tissue electrophysiology simulators using an n-version benchmark. Philos. Trans. R. Soc. A **369**, 4331–4351 (2011)
13. Ten Tusscher, K., Panfilov, A.: Cell model for efficient simulation of wave propagation in human ventricular tissue under normal and pathological conditions. Phys. Med. Biol. **51**, 6141 (2006)
14. Rognes, M.E., Farrell, P.E., Funke, S.W., Hake, J.E., Maleckar, M.C.M.: cbcbeat: an adjoint-enabled framework for computational cardiac electrophysiology. J. Open Source Softw. **2**, 224 (2017)
15. Alnæs, M.S., Blechta, J., Hake, J., et al.: The fenics project version 1.5. Arch. Numer. Softw. **3**, 9 (2015)
16. Viola, F., Meschini, V., Verzicco, R.: Fluid-structure-electrophysiology interaction (fsei) in the left-heart: a multi-way coupled computational model. Eur. J. Mech. B **79**, 212–232 (2020)
17. Muñoz-Cobo, J.L., Mendizábal, R., Miquel, A., et al.: Use of the principles of maximum entropy and maximum relative entropy for the determination of uncertain parameter distributions in engineering applications. Entropy **19**, 486 (2017)
18. Maceira, A.M., Cosín-Sales, J., Roughton, M., et al.: Reference left atrial dimensions and volumes by steady state free precession cardiovascular magnetic resonance. J. Cardiovasc. Magn. Reson. **12**, 65 (2010)
19. Hudsmith, L.E., Petersen, S.E., Francis, J.M., et al.: Normal human left and right ventricular and left atrial dimensions using steady state free precession magnetic resonance imaging. J. Cardiovasc. Magn. Reson. **7**, 775–782 (2005)
20. Keller, A., Gopal, A., King, D.: Left and right atrial volume by freehand three-dimensional echocardiography: in vivo validation using magnetic resonance imaging. Eur. J. Echocardiogr. **1**, 55–65 (2000)
21. Dössel, O., Krueger, M.W., Weber, F.M., et al.: Computational modeling of the human atrial anatomy and electrophysiology. Med. Biol. Eng. Comput. **50**, 773–799 (2012)
22. Hayashi, H., Lux, R.L., Wyatt, R.F., et al.: Relation of canine atrial activation sequence to anatomic landmarks. Am. J. Physiol.-Heart Circ. Physiol. **242**, H421–H428 (1982)
23. Pegolotti, L., Dedè, L., Quarteroni, A.: Isogeometric analysis of the electrophysiology in the human heart: numerical simulation of the bidomain equations on the atria. Comput. Methods Appl. Mech. Eng. **343**, 52–73 (2019)
24. Truex, R.C., Smythe, M.Q., Taylor, M.J.: Reconstruction of the human sinoatrial node. Anatom. Rec. **159**, 371–378 (1967)
25. Hurtado, D.E., Castro, S., Madrid, P.: Uncertainty quantification of 2 models of cardiac electromechanics. Int. J. Numer. Methods Biomed. Eng. **33**(12), e2894 (2017)
26. Sobol'Ilya, M., Shukhman, B.V.: On global sensitivity indices: Monte Carlo estimates affected by random errors. Monte Carlo Methods Appl. **13**, 89–97 (2007)
27. Gratiet, L.L., Marelli, S., Sudret, B.: Metamodel-Based Sensitivity Analysis: Polynomial Chaos Expansions and Gaussian Processes. Handbook of Uncertainty Quantification, pp. 1–37 (2016)
28. Caflisch, R.E.: Monte Carlo and quasi-monte Carlo methods. Acta Numer. **7**, 1–49 (1998)
29. Mohri, M., Rostamizadeh, A., Talwalkar, A.: Foundations of Machine Learning. MIT Press, Cambridge (2018)
30. Rousselet, G., Pernet, C., Wilcox, R.R.: A practical introduction to the bootstrap: a versatile method to make inferences by using data-driven simulations (2019)
31. Dubreuil, S., Berveiller, M., Petitjean, F., et al.: Construction of bootstrap confidence intervals on sensitivity indices computed by polynomial chaos expansion. Reliab. Eng. Syst. Saf. **121**, 263–275 (2014)
32. Blatman, G., Sudret, B.: Efficient computation of global sensitivity indices using sparse polynomial chaos expansions. Reliab. Eng. Syst. Saf. **95**, 1216–1229 (2010)
33. Pathmanathan, P., Cordeiro, J.M., Gray, R.A.: Comprehensive uncertainty quantification and sensitivity analysis for cardiac action potential models. Front. Physiol. **10**, 721 (2019)
34. Wilders, R., Jongsma, H., Van Ginneken, A.: Pacemaker activity of the rabbit sinoatrial node. a comparison of mathematical models. Biophys. J. **60**(5), 1202–1216 (1991)
35. Zhang, H., Holden, A., Kodama, I., et al.: Mathematical models of action potentials in the periphery and center of the rabbit sinoatrial node. Am. J. Physiol.-Heart Circul. Physiol. **279**, H397–H421 (2000)
36. Merckx, K.L., De Vos, C.B., Palmans, A., et al.: Atrial activation time determined by transthoracic doppler tissue imaging can be used as an estimate of the total duration of atrial electrical activation. J. Am. Soc. Echocardiogr. **18**, 940–944 (2005)
37. Quaglino, A., Pezzuto, S., Koutsourelakis, P.S., et al.: Fast uncertainty quantification of activation sequences in patient-specific cardiac electrophysiology meeting clinical time constraints. Int. J. Numer. Methods Biomed. Eng. **34**, e2985 (2018)
38. Lucor, D., Le Maître, O.P.: Cardiovascular modeling with adapted parametric inference. ESAIM **62**, 91–107 (2018)
39. Whittaker, D.G., Clerx, M., Lei, C.L., et al.: Calibration of ionic and cellular cardiac electrophysiology models. In: Wiley Interdisciplinary Reviews: Systems Biology and Medicine, p. e1482 (2020)
40. Roithinger, F.X., Abou-Harb, M., Pachinger, O., et al.: The effect of the atrial pacing site on the total atrial activation time. Pacing Clin. Electrophysiol. **24**, 316–322 (2001)
41. Ramirez, R.J., Nattel, S., Courtemanche, M.: Mathematical analysis of canine atrial action potentials: rate, regional factors, and electrical remodeling. Am. J. Physiol.-Heart Circ. Physiol. **279**, H1767–H1785 (2000)
42. Bueno-Orovio, A., Kay, D., Grau, V., et al.: Fractional diffusion models of cardiac electrical propagation: role of structural heterogeneity in dispersion of repolarization. J. R. Soc. Interface **11**, 20140352 (2014)
43. Cusimano, N., del Teso, F., Gerardo-Giorda, L., et al.: Discretizations of the spectral fractional Laplacian on general domains with Dirichlet, Neumann, and robin boundary conditions. SIAM J. Numer. Anal. **56**, 1243–1272 (2018)
44. Cusimano, N., Gizzi, A., Fenton, F., et al.: Key aspects for effective mathematical modelling of fractional-diffusion in cardiac electrophysiology: A quantitative study. Commun. Nonlinear Sci. Numer. Simul. **84**, 105152 (2020)

45. Meschini, V., Viola, F., Verzicco, R.: Modeling mitral valve stenosis: a parametric study on the stenosis severity level. J. Biomech. **84**, 218–226 (2019)
46. Nygren, A., Fiset, C., Firek, L., et al.: Mathematical model of an adult human atrial cell: the role of k+ currents in repolarization. Circ. Res. **82**, 63–81 (1998)
47. Seemann, G., Höper, C., Sachse, F.B., et al.: Heterogeneous three-dimensional anatomical and electrophysiological model of human atria. Philos. Trans. R. Soc. A **364**, 1465–1481 (2006)
48. Trayanova, N.A.: Whole-heart modeling: applications to cardiac electrophysiology and electromechanics. Circ. Res. **108**, 113–128 (2011)
49. Rodriguez, B., Trayanova, N., Noble, D.: Modeling cardiac ischemia. Ann. N.Y. Acad. Sci. **1080**, 395 (2006)
50. Seemann, G., Bustamante, P.C., Ponto, S., et al.: Atrial fibrillation-based electrical remodeling in a computer model of the human atrium. In: 2010 Computing in Cardiology, pp. 417–420. IEEE (2010)
51. Viola, F., Jermyn, E., Warnock, J., et al.: Left ventricular hemodynamics with an implanted assist device: an in vitro fluid dynamics study. Ann. Biomed. Eng. **47**(8), 1799–1814 (2019)
52. Rawles, J.M.: A mathematical model of left ventricular function in atrial fibrillation. Int J. Bio-medical Comput. **23**, 57–68 (1988)
53. Cherry, E.M., Fenton, F.H.: Suppression of alternans and conduction blocks despite steep apd restitution: electrotonic, memory, and conduction velocity restitution effects. Am. J. Physiol.-Heart Circul. Physiol. **286**, H2332–H2341 (2004)
54. Gizzi, A., Cherry, E., Gilmour Jr., R.F., et al.: Effects of pacing site and stimulation history on alternans dynamics and the development of complex spatiotemporal patterns in cardiac tissue. Front. Physiol. **4**, 71 (2013)
55. Meschini, V., Viola, F., Verzicco, R.: Heart rate effects on the ventricular hemodynamics and mitral valve kinematics. Comput. Fluids **197**, 104359 (2020)